Identification of a potent synthetic FXR agonist with an unexpected mode of binding and activation

Stephen M. Soisson*, Gopalakrishnan Parthasarathy, Alan D. Adams, Soumya Sahoo, Ayesha Sitlani, Carl Sparrow, Jisong Cui, and Joseph W. Becker

Merck Research Laboratories, POB 2000, Rahway, NJ 07065

Edited by John Kuriyan, University of California, Berkeley, CA, and approved February 6, 2008 (received for review November 19, 2007)

The farnesoid X receptor (FXR), a member of the nuclear hormone receptor family, plays important roles in the regulation of bile acid and cholesterol homeostasis, glucose metabolism, and insulin sensitivity. There is intense interest in understanding the mechanisms of FXR regulation and in developing pharmaceutically suitable synthetic FXR ligands that might be used to treat metabolic syndrome. We report here the identification of a potent FXR agonist (MFA-1) and the elucidation of the structure of this ligand in ternary complex with the human receptor and a coactivator peptide fragment using x-ray crystallography at 1.9-Å resolution. The steroid ring system of MFA-1 binds with its D ring-facing helix 12 (AF-2) in a manner reminiscent of hormone binding to classical steroid hormone receptors and the reverse of the pose adopted by naturally occurring bile acids when bound to FXR. This binding mode appears to be driven by the presence of a carboxylate on MFA-1 that is situated to make a salt-bridge interaction with an arginine residue in the FXR-binding pocket that is normally used to neutralize bound bile acids. Receptor activation by MFA-1 differs from that by bile acids in that it relies on direct interactions between the ligand and residues in helices 11 and 12 and only indirectly involves a protonated histidine that is part of the activation trigger. The structure of the FXR:MFA-1 complex differs significantly from that of the complex with a structurally distinct agonist, fexaramine, highlighting the inherent plasticity of the receptor.

NR1H4 | bile acid receptor | nuclear receptor | x-ray crystallography

The farnesoid X receptor (FXR) plays key roles in regulating cholesterol and bile acid homeostasis (1–4). Central to this function is the ability of bile acid-activated FXR to down-regulate the expression of Cyp7a (1, 5, 6), the rate-limiting step in the liver for the conversion of free cholesterol to bile acids, and the up-regulation of the bile salt excretion pump (BSEP), which functions to pump excess bile acids into the gall bladder for eventual fecal excretion (7). Treatment of *ob*/*ob* and *db*/*db* mice with the synthetic FXR agonist GW4064 significantly improves hypercholesterolemia (8) and lowers free fatty acids (9, 10) and triglyceride levels (11). Additional research has shown that $fxr^{-/-}$ mice show insulin resistance and impaired glucose tolerance (8, 10, 12), and that expression of constitutively active FXR in the liver results in hypoglycemia (10). Similarly, treatment with GW4064 increases insulin sensitivity in *ob*/*ob* and *db*/*db* mice (8, 10). As such, FXR agonists may have utility in treating metabolic syndrome, a clustering of cardiovascular risk factors characterized by dyslipidemia (elevated triglyceride and low HDL levels), insulin resistance, and poor glucose regulation. Several excellent reviews have summarized the current state of FXR understanding (13, 14) and help build the case for the development of FXR modulators for the treatment of diabetes and metabolic syndrome (15).

FXR belongs to the large structurally conserved family of steroid and nuclear hormone receptors (NHRs) that function as ligand-regulated transcription factors. These ≈45-kDa proteins consist of an N-terminal DNA-binding domain that targets the receptor to specific genes, coupled by a flexible linker to a ≈20-kDa ligand-binding domain (LBD) that binds small lipophilic hormones and serves as the transcriptional switch (16, 17). Regulation of transcription by NHRs is a complex process that relies on the ligand-dependent recruitment of different coregulatory proteins to a surface on the LBD that, in turn, mediate interactions with the basal transcriptional machinery, resulting in repression or activation of transcription (18). The binding of agonist ligands to the LBD induces a conformational change in the receptor that releases bound transcriptional corepressor proteins and creates a binding surface for coactivators (19–21). The binding of coactivators to the receptor is mediated by nuclear receptor interaction domains (NIDs) on the proteins that contain a conserved LXXLL sequence, and short peptides containing these elements are sufficient for recapitulating these binding interactions (22, 23). Before this work, crystal structures of the rat and human FXR LBDs were determined in complex with bile acids and a synthetic ligand, respectively (24, 25). We report here the identification of a potent synthetic FXR agonist designated Merck FXR agonist #1 (MFA-1). The structure of a ternary complex of the FXR LBD containing MFA-1 and a coactivator peptide, determined using x-ray crystallography, reveals the molecular basis for FXR activation by MFA-1.

Results

Identification of MFA-1. To identify new FXR agonists that could serve as the starting point for medicinal chemistry optimization, we developed a high-throughput assay to screen for ligand-induced coactivator recruitment to FXR that was based on homogeneous time-resolved fluorescence (HTRF) (26). The FXR HTRF assay is similar to assays that were developed in-house for the estrogen and PPAR receptors (27, 28). The assay was used to screen a library of approximately one million compounds and identified a potent agonist designated MFA-1 [17β-(4-hydroxybenzoyl)androsta-3,5-diene-3-carboxylic acid] (Fig. 1). Titration studies demonstrated that the compound has an EC_{50} of 16.9 nM in the coactivator recruitment assay (Fig. 2). MFA-1 is nearly 500-fold more potent than the highest-affinity naturally occurring bile acid agonist, chenodeoxycholic acid (CDCA), which has an EC_{50} of ≈8,300 nM. The potency of MFA-1 is comparable with that observed with GW4064 (Fig. 2), the most commonly reported synthetic FXR agonist in the literature (11). Fexaramine, another synthetic FXR agonist (24), is also reported to show an EC_{50} comparable to GW4064 in a

Author contributions: S.M.S. and G.P. designed research; S.M.S. and G.P. performed research; A.D.A., A.S., and J.C. contributed new reagents/analytic tools; S.M.S., A.D.A., S.S., A.S., C.S., J.C., and J.W.B. analyzed data; and S.M.S. wrote the paper.

The authors declare no conflict of interest.

This article is a PNAS Direct Submission.

Data deposition: The atomic coordinates have been deposited in the Protein Data Bank, www.pdb.org (PDB ID code 3BEJ).

*To whom correspondence should be addressed. E-mail: stephen_soisson@merck.com.

This article contains supporting information online at www.pnas.org/cgi/content/full/0710981105/DCSupplemental.

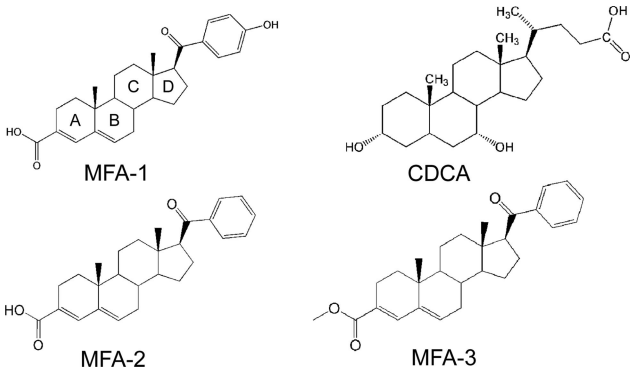

Fig. 1. FXR agonist ligands. The conventional steroid ring designations (A–D) are marked on MFA-1.

similar assay, suggesting that MFA-1 and fexaramine have similar EC_{50} values for coactivator recruitment.

Crystal Structure Determination. To understand the mechanism of receptor activation by MFA-1, we determined the crystal structure of the FXR LBD (residues 235–472) in complex with MFA-1 and a coactivator peptide derived from SRC-1. We noticed the purified protein was prone to time-dependent aggregation and precipitation, which could be due to oxidation of one or more of the four free cysteines present in the expressed fragment of FXR. To ameliorate this problem, we treated the protein with iodoacetic acid to covalently modify the free cysteines, and this modified protein greatly increased the reproducibility of crystallization. The crystals form in space group $P2_12_12_1$ with unit cell dimensions of $a = 40.1$, $b = 90.1$, and $c = 129.7$ Å and contain two ternary complexes in the asymmetric unit. Crystals of selenomethionyl-substituted protein were prepared, and the structure was experimentally determined by using a four-wavelength multiwavelength anomalous dispersion (MAD) experiment at 2.3-Å resolution (see *Materials and Methods*). The experimental electron-density maps were of high quality and allowed all features of the protein, including MFA-1 and the coactivator peptide [supporting information (SI) Figs. S1 and S2], to be modeled with confidence. The resultant model was refined against a native dataset at 1.9-Å resolution to generate the structure presented here (Table S1).

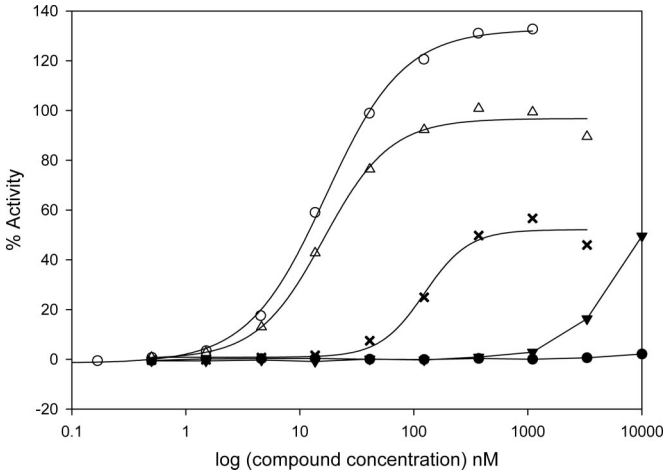

Fig. 2. Results of titration studies to determine compound EC_{50} values in a coactivator recruitment assay. The percentage maximal activity relative to a saturating concentration of CDCA (methods) is plotted as a function of ligand concentration. MFA-1 (open triangles), GW4064 (open circles), CDCA (solid triangles), MFA-2 (crosses), and MFA-3 (solid circles).

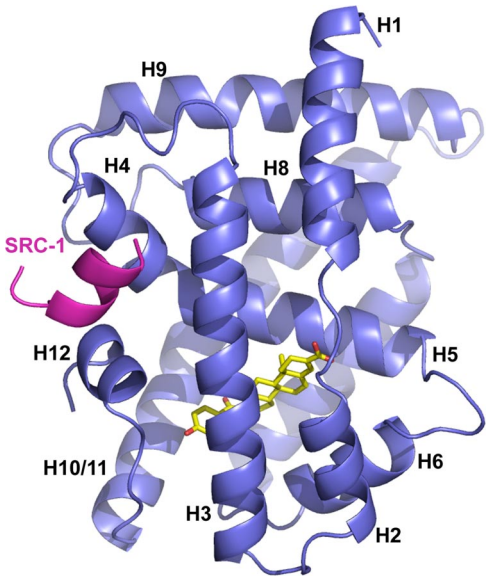

Fig. 3. Overall structure of human FXR (blue) in complex with MFA-1 (yellow) and an SRC-1 coactivator peptide (magenta). Helices discussed in the text are labeled H1-H12, for reference.

The structure of human FXR in complex with MFA-1 closely resembles the structures of rat and human FXR reported (24, 25), including the presence of a unique helix (helix 6) that replaces a β-turn structure seen in many other NHRs (Fig. S3). The structure has the overall structure characteristic of the NHR family, consisting of 12 helices folded into a compact globular domain that completely buries the lipophilic ligand in an appropriately sized cavity (Fig. 3). In this activated receptor structure, helix 12, also referred to as the activation function-2 domain (AF-2), is packed tightly against the body of the LBD in a manner similar to that observed in complexes with bile acids and fexaramine. In this structure, the binding of SRC-1 coactivator peptide to the receptor is extremely similar to the binding of the GRIP-1 peptide to rat FXR in response to bile acid binding (25) and therefore will not be discussed in detail here (Fig. S4).

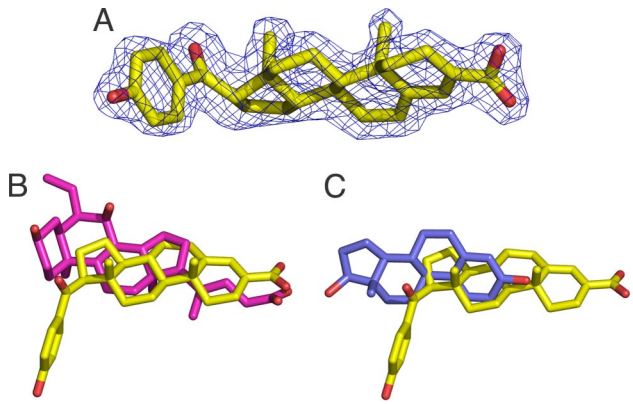

Fig. 4. General binding mode of MFA-1. (*A*) Final refined $2F_o-F_c$ electron density for MFA-1 contoured at 1.5 σ. (*B*) Results of the superposition of FXR molecules from the MFA-1(yellow) structure with rat FXR in complex with 6-ethyl-CDCA (magenta, PDB ID code 1OSV). The cα rmsd for the superposition is 1.177 Å. (*C*) Results of the superposition of FXR molecules from the MFA-1(yellow) structure with human ERβ in complex with estradiol (blue, PDB ID code 1QKT). The cα rmsd for the superposition is 4.217 Å.

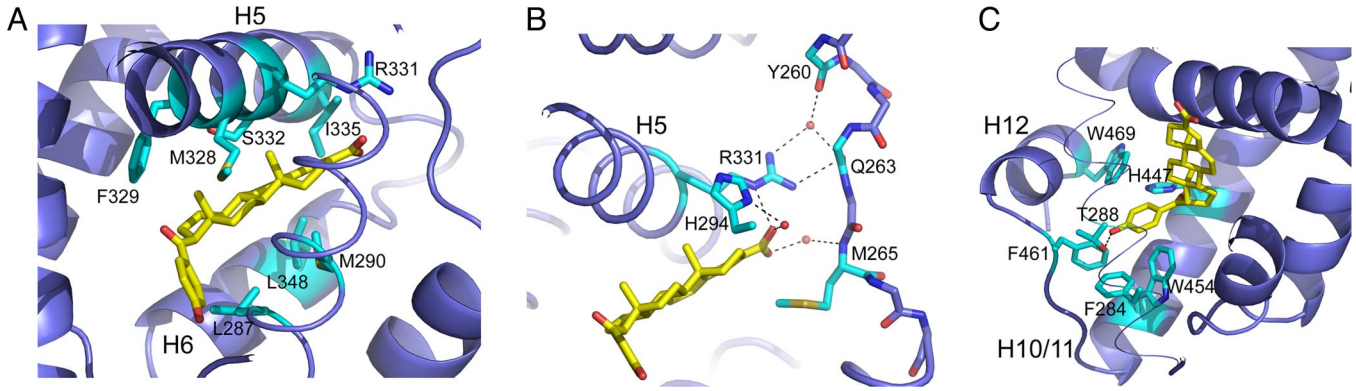

Fig. 5. Specific interactions between MFA-1 and FXR. (*A*) Interactions with the steroid ring system of MFA-1 (yellow). Side chains discussed in the text are colored cyan and labeled. (*B*) Stabilization of the helix 1–2 linker by MFA-1. Residues discussed in the text are labeled. (*C*) Stabilization of helix 12 by interactions with the hydroxy benzoyl group. Residues discussed in the text are colored cyan and labeled. Helix 3 is depicted as a thin trace for clarity.

MFA-1 Binds in a Flipped Orientation Relative to Bile Acids. Both the experimental (Fig. S2) and refined electron density (Fig. 4*A*) maps allowed unambiguous placement of MFA-1 into the structure. When compared with the aligned structure of FXR in complex with 6-ethyl-CDCA, a potent bile acid analog, it is clear that MFA-1 binds in a fundamentally different manner with its steroid ring rotated ≈180° relative to bile acid ligands (Fig. 4*B*). Overall, this binding mode is similar to that adopted by the "classical" steroid hormones, like estrogens and glucocorticoids, in binding to their receptors; however, superposition of the FXR:MFA-1 structure with the ERβ:estradiol structure (29) (Fig. 4*C*) shows that the estradiol ring system is translated and rotated significantly compared with the MFA-1 ring system, making detailed analogies between these classes of receptors unenlightening. The flipped binding mode places the D-ring of MFA-1 approximately where the B-ring of the bile acids would normally be positioned and also results in a superposition of the carboxylate group of MFA-1 (attached to the A-ring) with the carboxylate group extending from the D-ring of bile acids (Fig. 4*B*).

The steroid ring system of MFA-1 is sandwiched between two hydrophobic layers of residues contributed from helices 3, 5, and 6 (Fig. 5*A*). The observation that the steroid ring system adopts an orientation opposite to that seen with bile acids is somewhat surprising based on previous suggestions that FXR uses shape discrimination to preferentially bind bile acids over conventional steroids (25). The current results suggest that shape discrimination is not the only feature of the receptor dictating the binding mode of steroids to FXR, because MFA-1 also lacks the *cis* linkage between the A and B rings that is a unique feature of the bile acids (25), yet it is still bound efficiently by the receptor. Our results, coupled with the fact that the nonpolar surfaces of MFA-1 and bile acids are sandwiched between hydrophobic layers of residues in the receptor that are unlikely to provide binding specificity *per se*, makes it tempting to speculate that FXR does not discriminate among steroid rings and their binding orientation but rather uses other elements of the binding pocket to select ligands.

The carboxylate of MFA-1 is neutralized by interactions with R331, the same side chain used to counteract the negative charge of bound bile acids (Fig. 5*B*). This interaction immobilizes R331, allowing it to make both direct and water-mediated hydrogen bonds to the flexible linker between helices 1 and 2 (Fig. 5*B*). These interactions and van der Waals interactions between the steroid ring and M265 help stabilize the linker and contribute to the overall stability of the receptor. In addition, the carboxylate of MFA-1 makes a water-mediated hydrogen bond to H294, similar to that seen in the complexes with bile acids, demonstrating that it plays an analogous role to the bile acid carboxylate in receptor binding. Formation of the salt bridge with R331 is not absolutely essential for high-affinity binding of ligands to FXR, as evidenced by the fact that fexaramine, an uncharged molecule, exhibits very high affinity to the receptor (24), and that taurine- and glycine-conjugated bile acids lacking the free carboxylate also bind and activate FXR (2–4). Nonetheless, the presence of a formal negative charge on FXR ligands, such as MFA-1, is likely to play a major role in dictating the orientation of the ligand in the binding pocket as a result of the need to neutralize the buried charge.

Additional receptor stabilization is found at the opposite end of MFA-1, where the hydroxy benzoyl ring is situated in a deep pocket at the junction of helices 3, 11, and 12 (Fig. 5*C*). The aromatic benzoyl ring makes an edge-to-face stacking interaction with W454, whereas additional van der Waals contacts are made with F284 from helix 3 and F461 in the helix 11–12 linker and direct contacts with W469 on helix 12. Finally, the polar phenolic hydroxyl group makes a direct hydrogen bond to the side chain of T288 on helix 3, completing the network of tight ligand interactions that stabilize this portion of the complex's structure.

The large number of hydrophobic interactions observed between MFA-1 and FXR suggest these interactions are an important factor for MFA-1 binding; however, polar interactions clearly play an important role. An analog of MFA-1 lacking the phenolic hydroxyl (MFA-2, Fig. 1) shows a 30-fold decrease in activity (EC_{50} = 509 nM) in the coactivator recruitment assay (Fig. 2). Similarly, an analog where the formal charge of the carboxylate is removed through formation of a methyl ester, in addition to removal of the phenolic hydroxyl (MFA-3, Fig. 1), exhibits no detectable activity in the coactivator recruitment assay (Fig. 2). These results suggest that polar interactions and particularly the salt-bridge interaction between the carboxylate and R331 contribute significantly to the binding of MFA-1.

Mechanism of Receptor Activation. Nuclear receptors in the inactive unliganded state generally have a poorly ordered helix 12 or AF-2 domain (20, 30–32). Agonist-mediated activation results from helix 12 adopting a stable conformation where it is packed against the body of the LBD, often making direct contacts with the ligand, as seen with FXR and MFA-1. The ability of helix 12 to adopt the activated conformation arises from the overall stability that agonist ligands impart to the receptor, in particular by ordering helices 3, 11, and 12. MFA-1 confers stability to disparate portions of FXR, where the carboxylate group stabilizes the helix 1–2 linker; the steroid ring system directly stabilizes helices 3, 5, and 6; and the hydroxylated aromatic ring

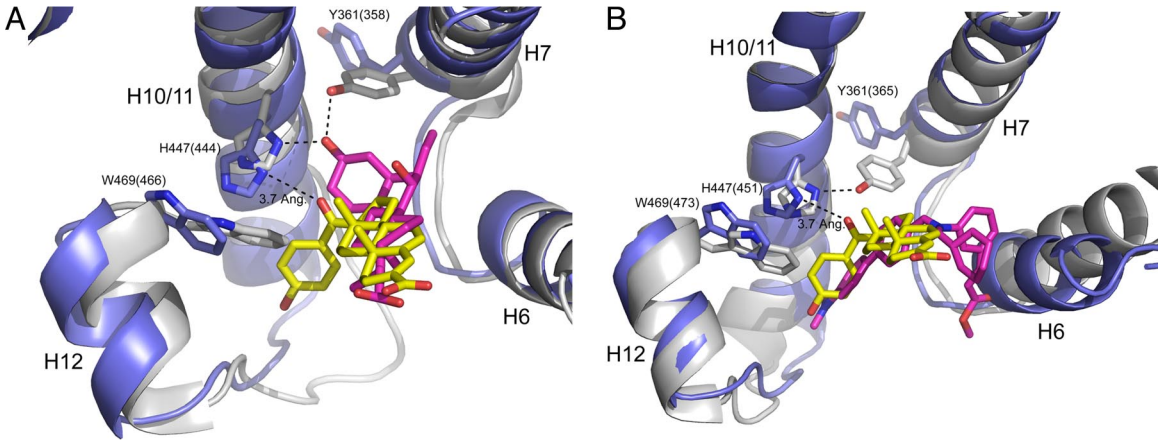

Fig. 6. Comparisons of the mechanism of receptor activation. (*A*) Alignment of the rat FXR (gray) structure in complex with 6-ethyl-CDCA (magenta) to the structure human FXR (blue) in complex with MFA-1 (yellow). Side chains discussed in the text are labeled and colored gray (rat FXR:6-ethyl CDCA), and blue (human FXR:MFA-1). Residue numbers in parentheses are for the rat receptor/6-ethyl-CDCA structure. (*B*) Alignment of the human FXR (gray) structure in complex with fexaramine (magenta, PDB ID code 1OSH) to the structure human FXR (blue) in complex with MFA-1 (yellow). Side chains discussed in the text are colored gray (human FXR:fexaramine), and blue (human FXR:MFA-1). Residue numbers in parentheses are for the fexaramine structure, and the $c\alpha$ rmsd for the superposition is 0.814 Å. Residue numbering differences arise from the use of different FXR isoforms that differ outside of the ligand binding domain contained in the crystal structures.

completes the molecular switch by stabilizing helix 12 in the active conformation. This overall stabilization likely plays a role in activation of the receptor, because NMR, deuterium exchange, and fluorescence anisotropy studies have shown that NHRs are poorly ordered in the absence of ligand, and that ligand-induced stabilization of the receptor correlates with activity (30, 31, 33).

MFA-1 activation of FXR is fundamentally different from the mechanism of bile acid-mediated activation. Alignment of the FXR:CDCA complex structure to the current structure with MFA-1 shows that the bile acids do not probe the helix 3,11,12 subpocket of the receptor (Fig. 6*A*). Instead, bile acid-mediated activation of FXR results from indirect stabilization of helix 12 through the formation of hydrogen bonds between the A-ring hydroxyl and Y361 and H447 (Fig. 6*A*). These interactions place the presumably protonated histidine in position to form a cation–π interaction with W469 on helix 12, stabilizing it in the active conformation (25). There are several key structural differences in the complex with MFA-1. The carbonyl oxygen linking the benzyl group to the steroid D ring is situated too far away (3.7 Å) to make direct hydrogen bonds with either H447 or Y361 (Fig. 6*A*). Receptor activation instead occurs through the direct contacts made with helices 3, 12, and the helix 11–12 linker. Positioning helix 12 and W469 in the activated conformation results in the formation of the same cation-π interaction between H447 and W469 observed in previously determined agonist-bound structures of FXR.

Fexaramine also activates the receptor through a direct helix 12 contact mechanism, because it makes no polar interactions with H447 but does probe the same subpocket between helices 3, 11, and 12 exploited by MFA-1 (Fig. 6*B*). In the fexaramine structure, Y361 is seen to form a direct hydrogen bond with H447, apparently substituting for the hydrogen bond that normally would be made by the A-ring hydroxyl of bile acids (Fig. 6). Interestingly, Y361 in the MFA-1 structure rotates out of the ligand-binding pocket. Although Y361 does not appear to be sterically occluded from occupying a conformation similar to that observed in the bile acid and fexaramine complexes, that helix 12 is pushed slightly further away from the LBD in the MFA-1 complex has the coordinated effect of pulling H447 away from the position where it can directly interact with Y361, as observed in the fexaramine complex. The lack of this direct hydrogen bond to H447 frees the tyrosine side chain to rotate out of the binding pocket.

Structural Plasticity of FXR. A comparison of the three known structures of FXR shows significant variation in the conformation of the receptor, suggesting that structural plasticity will likely complicate computational modeling and future structural studies of FXR. The human FXR:MFA-1 structure is most similar in conformation to the structure of the rat receptor with bound 6-ethyl-CDCA (Fig. 6); however, the previously discussed conformational change in Y361 creates a new subpocket in the ligand-binding site that could be exploited by appropriately modified MFA-1 analogs. The subtle difference in the positioning of W469 and helix 12 and that the coactivator peptide is still recruited to the receptor show there is some conformational permissiveness in what constitutes an active receptor. The most surprising differences are seen when comparing the current structure to of the FXR:fexaramine complex. Fexaramine appears to use an induced fit mechanism to interact with FXR, where helix 6 undergoes a significant change in position relative to the rest of the receptor (Fig. 6*B*) to create room for the tail-like extension of fexaramine. This tail would sterically clash with helix 6 in the conformation observed in both the bile acid and MFA-1 complexes (Fig. 6*B*). Interestingly, part of the helix 1–2 linker and all of helix 2 (Fig. 3) are completely disordered in the fexaramine complex. This disorder appears to be the result of the shift in position of helix 6; however, the implications of this disorder with regard to receptor function are not known. The same helix 1–2 linker is clearly observed in two distinct conformations when comparing the two monomers present in the structure presented here, suggesting that the linker is inherently flexible (see Fig. S5). It is also interesting to note there are five methionine residues in direct contact with MFA-1. The flexible nature of these side chains further suggests that the ligand-binding pocket of FXR may have considerable ability to accommodate differently shaped ligands.

Discussion

We describe here the identification of a potent synthetic FXR agonist called MFA-1 and characterization of the compound's mechanism of action using a coactivator recruitment assay and x-ray crystallography. The steroid ring system of MFA-1 binds in

a flipped orientation compared with the natural bile acid ligands, suggesting that the hydrophobic sandwich used by the receptor to bind the steroid ring system contributes little specificity to ligand binding. The steroid binding slot can likely accommodate a large variety of flat apolar ring systems, and the specificity and orientation of ligand binding are likely to be determined by how the compounds interact with other parts of the receptor, such as helix 12, and their ability to probe various subpockets present in the structures described thus far.

The structural plasticity of FXR discussed here is perhaps not surprising given the numerous precedents for the flexibility of LBDs in response to the binding of different ligands. For instance, recent studies with the androgen receptor show that side-chain rearrangements in the ligand-binding pocket can accommodate bulky extensions (34). Similarly, LXRβ undergoes binding-pocket rearrangements that allow two ligands that differ greatly in size and shape to bind with high affinity (35). Finally, both the vitamin D receptor and ecdysone receptors exhibit the apparent ability to bind different ligands in distinct yet partially overlapping binding pockets (36, 37). What is remarkable about the structural studies reported thus far is there are seemingly no common themes for this so-called receptor plasticity, making each distinct example of this phenomenon, with each receptor, extremely important for contributing to the general understanding of steroid and NHRs.

The structural variability seen in the three FXR structures described in the literature suggests that computational methods will have some difficulty in identifying novel FXR ligands and accurately predicting the details of their interactions with the receptor. This structural plasticity may also account for our experience with ligand-dependent FXR crystallization, a problem also alluded to in the structure report of the FXR:fexaramine complex. These difficulties will likely complicate future drug discovery efforts but also present great opportunities for exploring structurally diverse ligands of FXR with equally diverse gene activation profiles.

Materials and Methods

Protein Cloning, Expression, and Purification. The hFXRα4 ligand-binding domain (NP_005114; NM_005123), residues 235–472, was cloned in a pGEX-KG vector as described (38). This plasmid was transformed into the *Escherichia coli* strain BL21 and grown on LB agar plates supplemented with ampicillin (100 μg/ml). A single colony was used to inoculate 100 ml of LB medium and grown overnight at 37°C. Five liters of fresh LB media were inoculated with the overnight culture and grown at 37°C to an A_{600} of 0.7. Protein expression was induced with 1 mM isopropyl β-D-thiogalactoside, and growth continued for 18 h at 18°C. Cell pellets were harvested by centrifugation (6,000 $\times$ *g*, 15 min at 4°C), washed twice with PBS, and frozen at −80°C.

For purification, cell pellets were resuspended in cold lysis buffer (20 mM Tris, pH 8.0; 1 M NaCl; 1 mM DTT) and lysed by three passes through an Avestin Emulsiflex C-5 high-pressure homogenizer (Avestin). The crude lysate was clarified by centrifugation at 60,000 $\times$ *g* for 45 min at 4°C, and the supernatant was incubated with glutathione-Sepharose beads (Amersham Biosciences) that were preequilibrated with lysis buffer for 3 h. The suspension was washed with buffer (20 mM Tris, pH 8.0; 250 mM NaCl; 1 mM DTT) in a column, resuspended as slurry, and incubated with thrombin to release the FXR LBD from the GST fusion tag. Free FXR LBD was eluted from the beads with wash buffer and further purified by using MonoQ and Sephadex-75 columns. Purified FXR LBD was concentrated to 20 mg/ml, flash-frozen in liquid nitrogen, and stored at −80°C for further use. Preparation of selenomethionyl-substituted receptor and the carboxymethylation procedures are described in *SI Text*.

Crystallization and Data Collection. The FXR LBD was mixed with MFA-1 and a coactivator peptide containing residues 677–700 of SRC-1 (NP_003734.3; CPSSHSSLTERHKILHRLLQEGSPS), in a 1:5:5 molar ratio. The mixture was incubated on ice for 1 h, and the ternary complex was screened for crystallization by using the hanging-drop vapor diffusion method at room temperature. Each hanging droplet consisted of 1 μl of protein solution at 10 mg/ml (buffer: 20 mM Tris·HCl, pH 8.0; 50 mM NaCl) and 1 μl of the precipitating solution suspended over a 0.5-ml reservoir of the same precipitant. *De novo* microcrystals of the ternary complex grew in one condition (25% PEG3350; 0.2 M ammonium acetate; 0.1 M Bis-Tris buffer, pH 6.5) after 3 weeks. Further optimization yielded diffraction-quality crystals from a solution of 16–22% PEG3350; 0.1 M Bis-Tris, pH 6.5; 4 mM yittrium chloride; 0.2 M ammonium acetate; and 1 mM DTT. Crystals were cryoprotected before freezing in liquid nitrogen by sequential transfer to reservoir solutions containing increasing concentrations of ethylene glycol. Data were collected at 100 K in the facilities of the Industrial Macromolecular Crystallography Association (IMCA-CAT) located at the Advanced Photon Source (APS) in Argonne National Laboratories (Argonne, IL).

HTRF Coactivator Recruitment Assay. The HTRF-based coactivator recruitment assay was performed essentially as described in ref. 28; specific details related to the FXR assay can be found in *SI Text*.

Structure Determination. The crystal structure was experimentally determined via a four-wavelength MAD experiment by using crystals of the selenomethionyl-substituted FXR. Data were collected at low- and high-energy remote wavelengths, and the peak and inflection point energies were obtained from an EXAFS scan of the crystal. All 16 predicted Se atoms were found by using heavy atom search methods in SHELX (39), and initial experimental phases were calculated by using MLPHARE, as implemented in the CCP4 suite of programs (40). These phases were improved by using iterative rounds of SHARP phasing (41, 42) and solvent flattening to obtain a high-quality experimental electron density map. The initial model was subjected to simulated annealing refinement in CNX, followed by positional maximum-likelihood refinement in BUSTER/autoBUSTER (43). The final refined model contains residues 245–471 of monomer A, residues 244–471 of monomer B, 369 water molecules, one MFA-1 molecule, and one SRC-1 peptide bound per monomer (residues 628–638 visible). The final refined *R* and R_{free} values for the structure are 20.0% and 25.4%, respectively. The model has excellent geometry and stereochemistry, with 98% of residues in allowed regions of the Ramachandran plot. Coordinates and structure factors have been deposited with the Protein Data Bank (PDB ID code 3BEJ). All structure figures, including alignments, were prepared by using the program PyMOL (44).

ACKNOWLEDGMENTS. We thank Drs. Samuel Wright, Paula Fitzgerald, and Richard Ball for helpful discussions and Jinghua Yu for help in making FXR-LBD constructs, protein purification, and performance of FXR HTRF assays. We also thank Dr. Clemens Vonrhein of Global Phasing, Ltd. (Cambridge, U.K.) for help with phasing using SHARP. We thank the staff of IMCA-CAT at the Advanced Photon Source for valuable help with data collection. Use of the IMCA-CAT beamline 17-ID at the Advanced Photon Source was supported by the companies of the Industrial Macromolecular Crystallography Association through a contract with the Center for Advanced Radiation Sources at the University of Chicago.

1. Goodwin B, *et al.* (2000) A regulatory cascade of the nuclear receptors FXR, SHP-1, and LRH-1 represses bile acid biosynthesis. *Mol Cell* 6:517–526.
2. Makishima M, *et al.* (1999) Identification of a nuclear receptor for bile acids. *Science* 284:1362–1365.
3. Parks DJ, *et al.* (1999) Bile acids: natural ligands for an orphan nuclear receptor. *Science* 284:1365–1368.
4. Wang H, *et al.* (1999) Endogenous bile acids are ligands for the nuclear receptor FXR/BAR. *Mol Cell* 3:543–553.
5. Lu TT, *et al.* (2000) Molecular basis for feedback regulation of bile acid synthesis by nuclear receptors. *Mol Cell* 6:507–515.
6. Wang L, *et al.* (2002) Redundant pathways for negative feedback regulation of bile acid production. *Dev Cell* 2:721–731.
7. Ananthanarayanan M, Balasubramanian N, Makishima M, Mangelsdorf DJ, Suchy FJ (2001) Human bile salt export pump promoter is transactivated by the farnesoid X receptor/bile acid receptor. *J Biol Chem* 276:28857–28865.
8. Cariou B, *et al.* (2006) The farnesoid X receptor modulates adiposity and peripheral insulin sensitivity in mice. *J Biol Chem* 281:11039–11049.
9. Watanabe M, *et al.* (2004) Bile acids lower triglyceride levels via a pathway involving FXR, SHP, and SREBP-1c. *J Clin Invest* 113:1408–1418.
10. Zhang Y, *et al.* (2006) Activation of the nuclear receptor FXR improves hyperglycemia and hyperlipidemia in diabetic mice. *Proc Natl Acad Sci USA* 103:1006–1011.
11. Maloney PR, *et al.* (2000) Identification of a chemical tool for the orphan nuclear receptor FXR. *J Med Chem* 43:2971–2974.
12. Ma K, Saha PK, Chan L, Moore DD (2006) Farnesoid X receptor is essential for normal glucose homeostasis. *J Clin Invest* 116:1102–1109.
13. Lee FY, Lee H, Hubbert ML, Edwards PA, Zhang Y (2006) FXR, a multipurpose nuclear receptor. *Trends Biochem Sci* 31:572–580.
14. Kalaany NY, Mangelsdorf DJ (2006) LXRS and FXR: the yin and yang of cholesterol and fat metabolism. *Annu Rev Physiol* 68:159–191.

15. Cariou B, Staels B (2007) FXR: a promising target for the metabolic syndrome? *Trends Pharmacol Sci* 28:236–243.
16. Evans RM (1988) The steroid and thyroid hormone receptor superfamily. *Science* 240:889–895.
17. Mangelsdorf DJ, *et al.* (1995) The nuclear receptor superfamily: the second decade. *Cell* 83:835–839.
18. Rosenfeld MG, Lunyak VV, Glass CK (2006) Sensors and signals: a coactivator/corepressor/epigenetic code for integrating signal-dependent programs of transcriptional response. *Genes Dev* 20:1405–1428.
19. Nagy L, *et al.* (1999) Mechanism of corepressor binding and release from nuclear hormone receptors. *Genes Dev* 13:3209–3216.
20. Nagy L, Schwabe JW (2004) Mechanism of the nuclear receptor molecular switch. *Trends Biochem Sci* 29:317–324.
21. Shiau AK, *et al.* (1998) The structural basis of estrogen receptor/coactivator recognition and the antagonism of this interaction by tamoxifen. *Cell* 95:927–937.
22. McInerney EM, *et al.* (1998) Determinants of coactivator LXXLL motif specificity in nuclear receptor transcriptional activation. *Genes Dev* 12:3357–3368.
23. Nolte RT, *et al.* (1998) Ligand binding and co-activator assembly of the peroxisome proliferator-activated receptor-gamma. *Nature* 395:137–143.
24. Downes M, *et al.* (2003) A chemical, genetic, and structural analysis of the nuclear bile acid receptor FXR. *Mol Cell* 11:1079–1092.
25. Mi LZ, *et al.* (2003) Structural basis for bile acid binding and activation of the nuclear receptor FXR. *Mol Cell* 11:1093–1100.
26. Dickson EF, Pollak A, Diamandis EP (1995) Ultrasensitive bioanalytical assays using time-resolved fluorescence detection. *Pharmacol Ther* 66:207–235.
27. Zhou G, Cummings R, Hermes J, Moller DE (2001) Use of homogeneous time-resolved fluorescence energy transfer in the measurement of nuclear receptor activation. *Methods* 25:54–61.
28. Zhou G, *et al.* (1998) Nuclear receptors have distinct affinities for coactivators: characterization by fluorescence resonance energy transfer. *Mol Endocrinol* 12:1594–1604.
29. Gangloff M, *et al.* (2001) Crystal structure of a mutant hERalpha ligand-binding domain reveals key structural features for the mechanism of partial agonism. *J Biol Chem* 276:15059–15065.
30. Johnson BA, *et al.* (2000) Ligand-induced stabilization of PPARgamma monitored by NMR spectroscopy: implications for nuclear receptor activation. *J Mol Biol* 298:187–194.
31. Kallenberger BC, Love JD, Chatterjee VK, Schwabe JW (2003) A dynamic mechanism of nuclear receptor activation and its perturbation in a human disease. *Nat Struct Biol* 10:136–140.
32. Nettles KW, Greene GL (2005) Ligand control of coregulator recruitment to nuclear receptors. *Annu Rev Physiol* 67:309–333.
33. Bruning JB, *et al.* (2007) Partial Agonists Activate PPARgamma Using a Helix 12 Independent Mechanism. *Structure (London, UK)* 15:1258–1271.
34. Cantin L, *et al.* (2007) Structural characterization of the human androgen receptor ligand-binding domain complexed with EM5744, a rationally designed steroidal ligand bearing a bulky chain directed toward helix 12. *J Biol Chem* 282:30910–30919.
35. Farnegardh M, *et al.* (2003) The three-dimensional structure of the liver X receptor beta reveals a flexible ligand-binding pocket that can accommodate fundamentally different ligands. *J Biol Chem* 278:38821–38828.
36. Billas IM, *et al.* (2003) Structural adaptability in the ligand-binding pocket of the ecdysone hormone receptor. *Nature* 426:91–96.
37. Mizwicki MT, *et al.* (2004) Identification of an alternative ligand-binding pocket in the nuclear vitamin D receptor and its functional importance in 1alpha,25(OH)2-vitamin D3 signaling. *Proc Natl Acad Sci USA* 101:12876–12881.
38. Cui J, *et al.* (2002) The amino acid residues asparagine 354 and isoleucine 372 of human farnesoid X receptor confer the receptor with high sensitivity to chenodeoxycholate. *J Biol Chem* 277:25963–25969.
39. Weeks CM, *et al.* (2003) Automatic solution of heavy-atom substructures. *Methods Enzymol* 374:37–83.
40. Collaborative Computational Project No. 4 (1994) The CCP4 Suite: Programs for Protein Crystallography. *Acta Crystallogr D* 50:760–763.
41. delaFortelle E, Bricogne G (1997) Maximum-likelihood heavy-atom parameter refinement for multiple isomorphous replacement and multiwavelength anomalous diffraction methods. *Methods Enzymol* 276:472–494.
42. Vonrhein C, Blanc E, Roversi P, Bricogne G (2007) Automated structure solution with autoSHARP. *Methods Mol Biol* 364:215–230.
43. Roversi P, Blanc E, Vonrhein C, Evans G, Bricogne G (2000) Modelling prior distributions of atoms for macromolecular refinement and completion. *Acta Crystallogr D* 56:1316–1323.
44. DeLano WL (2002) *The Pymol Molecular Graphics System* (www.pymol.org).